J Biomol NMR (2012) 53:181–190
DOI 10.1007/s10858-012-9650-5

ARTICLE

^{13}C relaxation experiments for aromatic side chains employing longitudinal- and transverse-relaxation optimized NMR spectroscopy

Ulrich Weininger · Carl Diehl · Mikael Akke

Received: 25 December 2011 / Accepted: 21 March 2012 / Published online: 3 July 2012

Abstract Aromatic side chains are prevalent in protein binding sites, perform functional roles in enzymatic catalysis, and form an integral part of the hydrophobic core of proteins. Thus, it is of great interest to probe the conformational dynamics of aromatic side chains and its response to biologically relevant events. Indeed, measurements of ^{13}C relaxation rates in aromatic moieties have a long history in biomolecular NMR, primarily in the context of samples without isotope enrichment that avoid complications due to the strong coupling between neighboring ^{13}C spins present in uniformly enriched proteins. Recently established protocols for specific ^{13}C labeling of aromatic side chains enable measurement of ^{13}C relaxation that can be analyzed in a straightforward manner. Here we present longitudinal- and transverse-relaxation optimized pulse sequences for measuring R_1, R_2, and $\{^1H\}$–^{13}C *NOE* in specifically ^{13}C-labeled aromatic side chains. The optimized R_1 and R_2 experiments offer an increase in sensitivity of up to 35 % for medium-sized proteins, and increasingly greater gains are expected with increasing molecular weight and higher static magnetic field strengths. Our results highlight the importance of controlling the magnetizations of water and aliphatic protons during the relaxation period in order to obtain accurate relaxation rate measurements and achieve full sensitivity enhancement. We further demonstrate that potential complications due to residual two-bond ^{13}C–^{13}C scalar couplings or dipolar interactions with neighboring ^{1}H spins do not significantly affect the experiments. The approach presented here should serve as a valuable complement to methods developed for other types of protein side chains.

Keywords Relaxation · Protein dynamics · Aromatic side chain · Sensitivity enhancement · TROSY

Introduction

Protein dynamics plays a key role in protein function, including ligand binding, enzyme catalysis, and signal transduction. NMR spectroscopy is a powerful technique for studying such dynamic processes with high resolution across a wide range of time scales, extending from picoseconds to seconds or longer (Palmer 2004; Igumenova et al. 2006). The majority of studies published to date have focused on backbone dynamics through measurement of ^{15}N spin relaxation parameters (Jarymowycz and Stone 2006), but the critical role of side chains in mediating protein function has spawned the development of relaxation methods for methyl groups (Palmer et al. 1993; Muhandiram et al. 1995; Ishima et al. 2001; Millet et al. 2002), methylene groups (Yang et al. 1998), side-chain amides (Boyd 1995), carboxylates/carbonyls (Paquin et al. 2008), secondary amines of arginine and tryptophan (Berglund et al. 1995), and primary amines of lysines (Iwahara et al. 2007).

Aromatic residues occur frequently in the binding interfaces of proteins (Lo Conte et al. 1999). In particular, Tyr and Trp are overrepresented in "hot spots" that contribute a large fraction of the binding free energy (Bogan and Thorn 1998), Tyr is prevalent in antigen-binding sites

Electronic supplementary material The online version of this article (doi:10.1007/s10858-012-9650-5) contains supplementary material, which is available to authorized users.

U. Weininger · C. Diehl · M. Akke (✉)
Center for Molecular Protein Science, Department of Biophysical Chemistry, Lund University,
P.O. Box 124, 22100 Lund, Sweden
e-mail: mikael.akke@bpc.lu.se

of antibodies (Lo Conte et al. 1999; Birtalan et al. 2010), and His and Tyr play prominent roles in enzyme catalysis (Bartlett et al. 2002). Thus, it is of great interest to monitor the dynamics of aromatic side chains and changes in this dynamics upon formation of biologically relevant complexes. Furthermore, aromatic residues constitute a significant volume fraction (roughly 25 %) of the protein interior, and therefore represent an attractive complement to methyl-containing residues (which correspond to ca. 50 % of the core) as probes of the dynamics of the hydrophobic core (Wüthrich and Wagner 1975). Previous applications of ^{13}C relaxation have indicated that aromatic side chains show a rich variation in dynamics (Palmer et al. 1993), and theoretical considerations have predicted that ^{13}C relaxation rates should be quite sensitive to the motions of aromatic side chains (Levy and Sheridan 1983).

Relaxation experiments on uniformly ^{13}C-enriched aromatic side chains are seriously hampered by the strong *J*-coupling between neighboring sites in the aromatic rings. Labeling using 1-$^{13}C_1$- or 2-$^{13}C_1$-glucose solves the problem by creating isolated ^{13}C sites in aromatic side chains, i.e. sites that do not have any ^{13}C–^{13}C one-bond couplings (Teilum et al. 2006; Lundström et al. 2007). Specifically, labeling with 1-$^{13}C_1$-glucose introduces isolated ^{1}H–^{13}C pairs at the Cδ positions of Phe and Tyr, the Cδ1 and Cε3 of Trp, and the Cδ2 and Cε1 of His, while 2-$^{13}C_1$-glucose yields ^{13}C at the Cε positions of Phe and Tyr, and the Cζ3 and Cζ2 of Trp. Thus, the approach results in two complementary labeling patterns of isolated ^{13}C–^{1}H spin pairs suitable for canonical inverse-detected heteronuclear relaxation experiments similar to those developed for ^{15}N spins (Teilum et al. 2006; Boyer and Lee 2008; Sapienza et al. 2011).

However, it is evident that relaxation studies of aromatic ^{13}C spin systems can benefit from further pulse sequence optimization to achieve higher sensitivity. Specifically ^{13}C-labeled protein samples produced using $^{13}C_1$-glucose are limited in sensitivity by the resulting incorporation level of 50 % (Teilum et al. 2006; Lundström et al. 2007). The inherently fast transverse relaxation of aromatic ^{13}C spins, due in part to their sizeable chemical shift anisotropy (CSA), further reduces the relative sensitivity of these experiments; for example, R_2 is roughly a factor of 4 greater than that of backbone ^{15}N spins. Furthermore, His and Trp residues contain exchangeable protons vicinal to the ^{1}H–^{13}C pairs of interest; chemical exchange of these protons with water might cause differential effects on the intensities of the ^{1}H–^{13}C cross-peaks as a function of the relaxation delay, unless special care is taken to maintain the equilibrium magnetization of water throughout the relaxation period.

Here we present pulse sequences for aromatic ^{13}C relaxation experiments (R_1, R_2 and steady-state {^{1}H}–^{13}C *NOE*) that include longitudinal-relaxation optimization (Pervushin et al. 2002) and either TROSY (Pervushin et al. 1997, 1998) or PEP-HSQC approaches (Palmer et al. 1991; Kay et al. 1992). As part of these developments, we also demonstrate that neither the two-bond *J* couplings between ^{13}C spins, nor the dipolar interactions with remote or vicinal protons, adversely affect the relaxation data. The pulse sequences were tested on the carbohydrate binding domain of galectin-3 (Gal3C), which contains all four types of aromatic side chains: Phe, Tyr, Trp, and His. The experiments presented here significantly improve the sensitivity and overall performance compared to 'standard' experiments, enabling robust and efficient investigation of aromatic side chain relaxation.

Materials and methods

Expression and purification

The galectin-3 carbohydrate recognition domain (Gal3C; amino acid residues 113–250) was expressed and purified as described previously (Diehl et al. 2009, 2010) using M9 minimal medium containing either 100 % 1-$^{13}C_1$-glucose, or 50 % 1-$^{13}C_1$-glucose + 50 % $^{12}C_6$-glucose as the sole carbon source. In addition, one partially deuterated sample was produced using M9 minimal medium containing 100 % 1-$^{13}C_1$-glucose in 60 % D_2O.

NMR experiments

All NMR spectra were recorded on a Varian DirectDrive 500 MHz spectrometer at 298 K using 0.8 mM Gal3C samples in 5 mM HEPES pH 7.4 and 7 % D_2O. Shaped pulses were created using Pbox. Excitation and flip-back ^{1}H EBURP2 pulses (Geen and Freeman 1991) had a bandwidth of 3,300 Hz (6.6 ppm) and offset of −1,400 Hz (−2.8 ppm) from the water resonance. ^{1}H i-SNOB-5 pulses (Kupce et al. 1995) had a bandwidth of 1,350 Hz (2.7 ppm) and offset of 1,250 Hz (2.5 ppm), and ^{13}C REBURP pulses (Geen and Freeman 1991) had a bandwidth of 5,000 Hz (40 ppm). The ^{1}H carrier was set on the water frequency, while the ^{13}C carrier was centered in the aromatic region. For non-L-optimized control experiments the ^{1}H EBURP2 pulses were omitted, the ^{1}H i-SNOB-5 pulses were replaced by rectangular hard pulses, and the water resonance was suppressed using a 3–9–19 WATERGATE sequence (Sklenar et al. 1993).

^{1}H decoupling was applied during the relaxation delays using a series of ^{1}H i-SNOB-5 pulses. In the R_1 experiment, these pulses were spaced 50 ms apart, while in the R_2 experiment they were applied in the center of an 8 ms CPMG block consisting of 8 refocusing pulses that were

phase cycled as described previously (Yip and Zuiderweg 2004). Proton saturation in the $\{^1H\}$–^{13}C *NOE* experiment was achieved using a train of 180° pulses spaced by 20 ms delays (Ferrage et al. 2008, 2009). Relaxation data were acquired by interleaving relaxation delays and t_1 time points.

Data analysis

Spectra were processed using NMRpipe (Delaglio et al. 1995) and analyzed using NMRview (Johnson and Blevins 1994). Errors in the peak intensitites were estimated from the baseplane noise and duplicate data points. Relaxation data were fittted to mono-exponential decays. Errors in the fitted relaxation rate constants were estimated from the covariance matrix of the Levenberg–Marquardt fitting.

Results and discussion

Pulse sequences

In an effort to optimize the sensitivity of aromatic ^{13}C relaxation experiments, we implemented improved pulse sequences for the measurement of the longitudinal relaxation rate (R_1), the transverse relaxation rate (R_2), and the $\{^1H\}$–^{13}C *NOE*, which commonly form the basis for spectral density mapping or model-free analysis of protein dynamics.

The pulse sequences for the R_1, R_2, and $\{^1H\}$–^{13}C *NOE* experiments are shown in Fig. 1. Each relaxation experiment was implemented in the framework of either ^1H–^{13}C PEP-HSQC or ^1H–^{13}C TROSY-HSQC spectra (Fig. 1d–e). The INEPT transfer delays were tuned to a ^1H–^{13}C coupling constant of $^1J_{HC} = 155$ Hz, which yields near-optimal transfer for most aromatics, except for the Cε1 position of His, which has $^1J_{HC} > 200$ Hz.

Longitudinal relaxation optimization (L-optimization) involves maintaining the water and aliphatic magnetizations along the +z axis whenever possible (see further below). This was achieved by implementing selective flip-back of the water and aliphatic ^1H spins using EBURP2 pulses (Geen and Freeman 1991), as previously applied in the context of the L-GFT-TROSY experiment for aromatic rings (Eletsky et al. 2005). Furthermore, the selective ^{13}C REBURP pulse (Geen and Freeman 1991) in the first INEPT transfer step refocuses only the aromatic carbons to prevent the evolution of ^1H–^{13}C couplings of aliphatics in the first INEPT and make possible the re-alignment all aliphatic ^1H magnetization back to +z along with the water. The 180° pulses on ^1H during the relaxation delays of the R_1 and R_2 experiments and the saturation pulse train

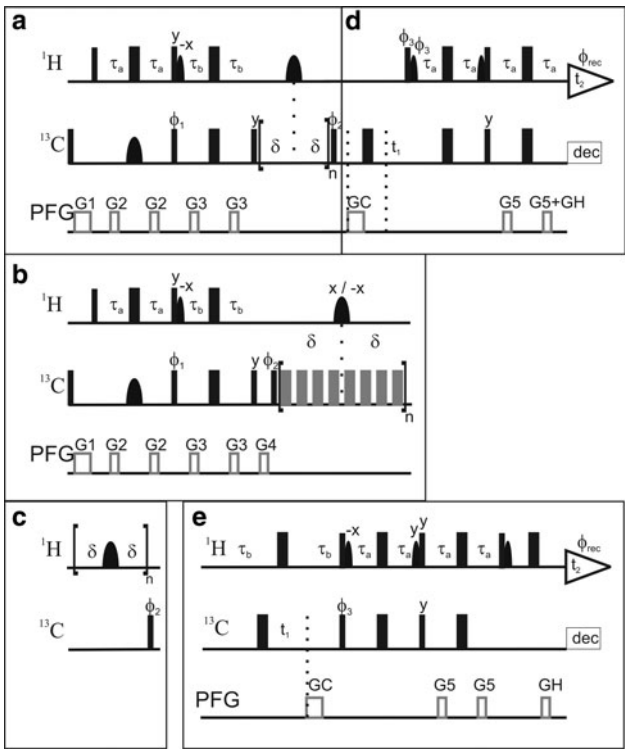

Fig. 1 L-optimized pulse sequences for measuring aromatic ^{13}C relaxation parameters. The pulse sequence of the R_1 relaxation experiment shown in the *top panel* is divided into two blocks that encode: **a** polarization transfer from ^1H to ^{13}C and the relaxation period; and **d** the ^{13}C evolution period followed by polarization transfer back to ^1H. The R_2 experiment is obtained by replacing *block a* with *block b*, and similarly the $\{^1H\}$–^{13}C *NOE* experiment is given by *block c*. The TROSY transfer sequence of *block d* can be substituted for the PEP-HSQC sequence given in *block e*. Each of the three relaxation experiments specified by *blocks a–c* can be combined with either of *blocks d* or *e*. *Narrow (wide) filled bars* represent 90° (180°) rectangular high power pulses. *Grey wide bars* in *block b* represent 180° rectangular CPMG pulses attenuated by 6 dB compared to the other hard pulses. *Filled bell-shaped bars* represent shaped pulses. *Narrow bell-shaped bars* on ^1H represent EBURP2 shapes (bandwidth of 6.6 ppm, shifted 2.8 ppm upfield), while *wide bell-shaped bars* are i-SNOB-5 pulses (bandwidth of 2.7 ppm, shifted 2.5 ppm downfield). *Wide bell-shaped* pulses on ^{13}C represent REBURP shapes (bandwidth 40 ppm). Pulsed field gradients (PFG) are indicated as *grey open bars*. Phases are *x* unless otherwise indicated. In all sequences $\tau_a = 1.5$ ms and $\tau_b = 1.623$ ms. The delay δ varies between blocks: in *a*, $\delta = 25$ ms; in *b*, $\delta = 4$ ms; and in *c*, $\delta = 10$ ms. In all experiments echo/anti-echo selection were made during t_1 by reversing ϕ_3, GC, and the even-numbered increments of ϕ_{rec}. For every second t_1 increment ϕ_2 and ϕ_{rec} were incremented. Durations and strengths of the gradients are G1 = (1 ms, 10 G/cm); G2 = (0.5 ms, 8 G/cm); G3 = (0.5 ms, 12 G/cm); G4 = (0.5 ms, 16 G/cm), G5 = (0.5 ms, 18 G/cm), GC = (1 ms, −50 G/cm), GH = (0.5 ms, 25 G/cm). The phase cycling for the different experiments is: a + d and b + d, ϕ_1 = (x, x, x, x, −x, −x, −x, −x), ϕ_2 = (y, x, −y, −x), ϕ_{rec} = (x, −y, −x, y, −x, y, x, −y); c + d, ϕ_2 = (y, x, −y, −x), ϕ_{rec} = (x, −y, −x, y); a + e and b + e, ϕ_1 = (x, x, −x, −x), ϕ_2 = (y, −y), ϕ_{rec} = (x, −x, −x, x); c + e, ϕ_2 = (y, −y), ϕ_{rec} = (x, −x). The phase cycling within the CPMG block is (x, x, y, −y, x, x, −y, y) in b + e, and (y, y, −x, x, y, y, x, −x) in b + d. The phase of the shaped ^1H pulse in middle of the CPMG block is x for CPMG block n and −x for n + 1

of the *NOE* experiment were implemented as i-SNOB-5 pulses (Kupce et al. 1995) selective for the aromatic region.

In the R_2 experiment (Fig. 1b) an additional gradient (G4) was added before the CPMG block, in order to purge non-refocused magnetization arising as a consequence of the non-uniform ^{1}H–^{13}C coupling constants in aromatic side chains. Off-resonance artefacts of the CPMG refocusing pulses were suppressed by the phase cycle proposed by Yip and Zuiderweg (2004). ^{1}H saturation in the $\{^{1}H\}$–^{13}C *NOE* experiment was achieved using 180° pulses as described (Ferrage et al. 2008, 2009). TROSY selection (Fig. 1d) was implemented in the ^{13}C dimension only (Pervushin et al. 1998), which allows for a simplified TROSY scheme (Eletsky et al. 2005). In the following we describe key aspects of these pulse sequences.

TROSY versus PEP-HSQC detection in specifically ^{13}C-labeled proteins

TROSY detection of aromatic resonances has been shown to be advantageous in experiments developed for uniformly ^{13}C-labeled proteins (Pervushin et al. 1998). Calculations based on the chemical shift tensor of benzene ($\sigma_{11} = 225$ ppm, $\sigma_{22} = 149$ ppm, and $\sigma_{33} = 15$ ppm; Veeman 1984) indicate that the TROSY effect is close to optimal at a static magnetic field strength of 14.1 T, and provides significant sensitivity enhancement at field strengths from 11.7 to 18.8 T (Pervushin et al. 1998). The chemical shift tensors of tryptophan Cδ1 ($\sigma_{11} = 202$, $\sigma_{22} = 121$, and $\sigma_{33} = 48$ ppm; Separovic et al. 1991) and Cε3 ($\sigma_{11} = 208$, $\sigma_{22} = 137$, and $\sigma_{33} = 15$ ppm; Separovic et al. 1999) are comparable to that of benzene, indicating similar TROSY effects for these sites.

Experiments for uniformly ^{13}C-labeled samples include a constant-time evolution period (17.6 ms) to refocus one-bond ^{13}C–^{13}C couplings (Pervushin et al. 1998), which incurs a significant loss in sensitivity. By contrast, in specifically ^{13}C-labeled proteins, the one-bond ^{13}C–^{13}C couplings are eliminated and the evolution period can be kept quite short due to the narrow frequency range of the aromatic region of the ^{13}C spectrum. We tested both TROSY and PEP-HSQC approaches with either constant-time or non-constant time evolution periods on Gal3C at different global correlation times (τ_c) by varying the temperature (Supplementary Fig. S1). The non-constant time PEP-HSQC experiment is more sensitive than the TROSY up to a global correlation time of about 13 ns (corresponding to a molecular weight of approximately 16 kDa at 5 °C), but the TROSY version results in narrower linewidths, as expected. We note that the inherent reduction in sensitivity that results from 1- or 2-$^{13}C_1$-glucose labeling (50 % incorporation) is essentially compensated for by the increase in sensitivity that results from the shortened t_1 evolution period of the non-constant time experiment. Thus, aromatic ^{1}H–^{13}C correlation spectra of medium-sized and $^{13}C_1$-glucose-labeled proteins have comparable sensitivities to those obtained using constant-time TROSY spectroscopy on uniformly ^{13}C-enriched samples (Pervushin et al. 1998), thereby making the former samples very well suited also for other purposes than relaxation studies.

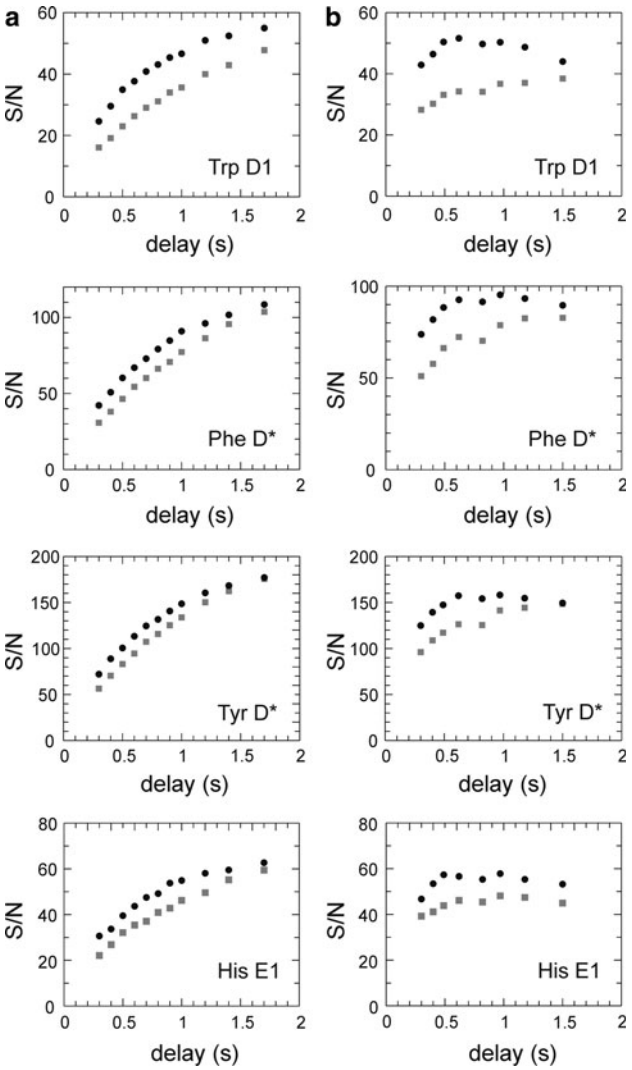

Fig. 2 Sensitivity (signal-to-noise ratio, S/N) versus length of the recovery delay for L-optimized (*black circles*) and non-L-optimized (*grey squares*) versions of the R_1 pulse sequence. Representative data are shown for different aromatic ^{13}C sites (Trp181 Cδ1, Phe163 Cδ*, Tyr247 Cδ*, and His208 Cε1). **a** data acquired with a constant number of transients. **b** data acquired with a constant total experiment time. An optimal recovery time was estimated to 0.6 s for L-optimized and 1.5 s for non-optimized versions (*right-hand column*). The average gain in S/N for L-optimization is 35 % (Trp Cδ1), 10 % (Phe Cδ*), 10 % (Tyr Cδ*), and 25 % (His Cε1). Similar results are obtained for the R_2 experiment

Longitudinal relaxation optimization

In L-optimized spectroscopy (Pervushin et al. 2002), ^{1}H spins not used for polarization transfer and detection are maintained close to equilibrium (i.e. magnetization along +z) throughout the experiment, including the relaxation, t_1 evolution, and acquisition periods. This unperturbed "thermal bath" leads to efficient relaxation of the detected protons, as is well illustrated by comparing the effective relaxation rates in selective versus non-selective inversion recovery experiments (Cavanagh et al. 2007). Thus, L-optimization enables the use of shorter recycle delays and hence improved sensitivity in terms of signal-to-noise (S/N) per unit time. L-optimization is achieved using shaped, frequency-selective pulses to control the aromatic ^{1}H spins separately from the water and aliphatic ^{1}H spins. As described in more detail below, this level of control is critical in any type of quantitative experiment that starts from a non-equilibrium state and involves variable relaxation delays.

We investigated the benefits of L-optimization by comparing with non-L-optimized pulse sequences. Figure 2a shows the signal-to-noise ratio (S/N) as a function of recovery delay in the R_1 experiment. To find the optimal recovery delay with respect to S/N, we repeated both the L-optimized and non-L-optimized experiments using the same total experimental time for each measured point (Fig. 2b). The optimal recovery time for L-optimized experiments of aromatics was determined to be 0.6 s for Gal3C. The average gain in S/N achieved with L-optimization was 10 % for Phe and Tyr Cδ*, 25 % for His Cδ2 and Cε1, and 35 % for Trp Cδ1. The additional increase in S/N observed for Trp and His is most probably caused by the presence of exchangeable protons vicinal to the ^{13}C sites in question; exchange of these protons for water protons with near-equilibrium magnetization provides an efficient relaxation mechanism for the protons attached to the labeled carbons. The increased S/N is particularly useful in the context of 1-$^{13}C_1$- or 2-$^{13}C_1$-glucose labeling, which restricts the level of ^{13}C incorporation to 50 %, and consequently limits the overall sensitivity of these samples. Phe and Tyr usually have inherently higher sensitivity due to the presence of two chemically identical carbons that contribute to the same peak intensity whenever the two resonances are averaged by rapid ring flips. Thus, L-optimization preferentially augments those side chains (Trp

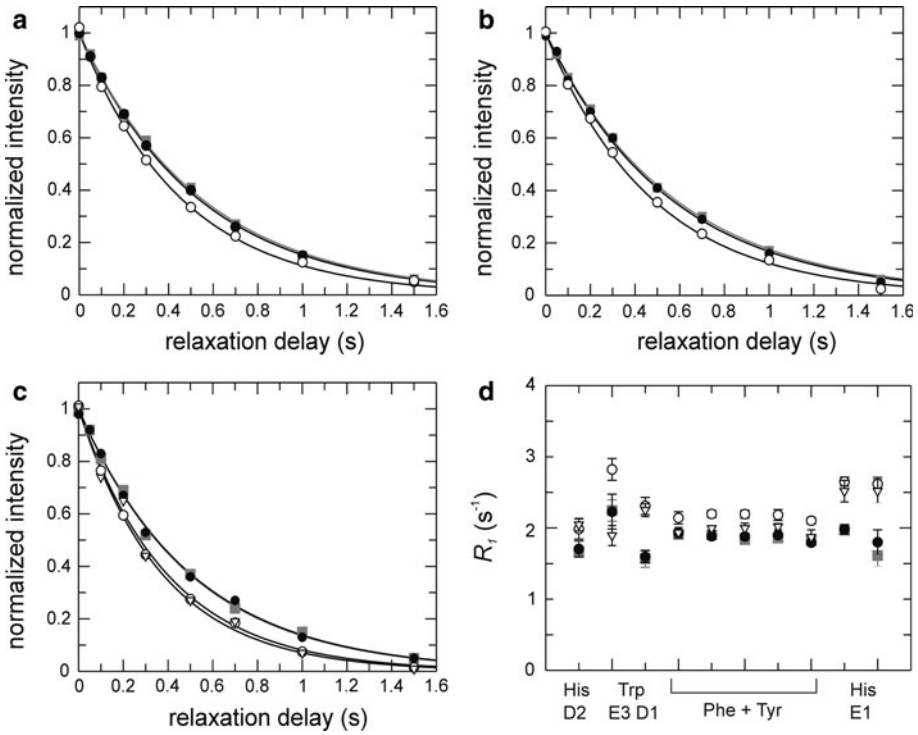

Fig. 3 Dependence of R_1 on the treatment of the ^{1}H magnetization during the variable relaxation delay. **a**–**c** Representative relaxation decays (**a** Phe163 Cδ*; **b** Phe190 Cδ*; **c** His208 Cε1) obtained using pulse sequences without (*grey squares*) or with L-optimization using selective i-SNOB-5 (*black circles*) or non-selective (*open circles*) ^{1}H inversion pulses during the relaxation delay. Panel **c** includes data obtained using rectangular ^{1}H inversion pulses in combination with water flip-back (*open triangles*). **d** R_1 rate constants obtained with the different implementations for different types of aromatic side chains, from *left* to *right*: His222 Cδ2, Trp181 Cε3, Trp181 Cδ1, Phe198 Cδ*, Phe149 Cδ* + Phe159 Cδ* + Tyr118 Cδ* + Tyr221 Cδ*, Phe163 Cδ*, Phe192 Cδ*, Phe209 Cδ*, His158 Cε1, and His217 Cε1. The non-L-optimized experiment utilized a recycle delay of 3.8 s

and His) that have the lowest inherent sensitivity, thereby making the signal intensities from the different aromatic sites more uniform on average. This result contrasts with what is observed for ^{1}H–^{15}N correlated experiments, where L-optimization typically leads to a less uniform distribution of signal intensities (Pervushin et al. 2002).

We next verified that the L-optimized pulse sequences yield accurate relaxation rates. Figure 3a–c show a

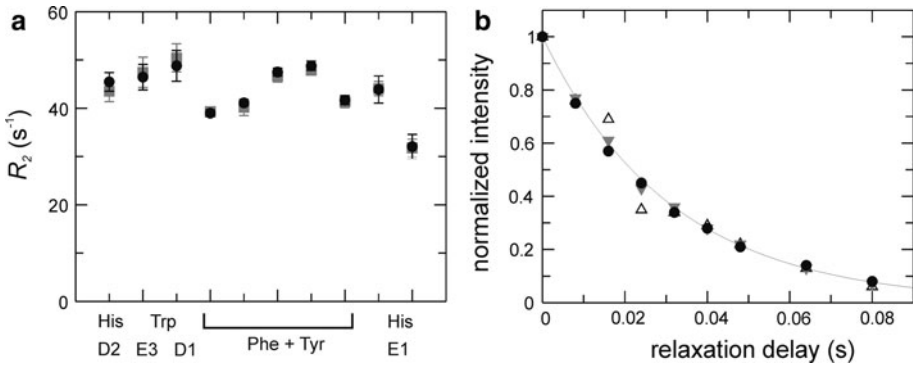

Fig. 4 R_2 CPMG in-phase relaxation experiment. **a** R_2 rate constants for different types of aromatic ^{13}C sites determined using L-optimized (*black circles*) and non-L-optimized (*grey squares*) experiments. **b** Relaxation decays for His $^{13}C\varepsilon1$ obtained with $\tau_b = 1.623$ ms (tuned to $^{1}J_{HC} = 154$ Hz) and the purge gradient G4 included (*filled circles*), or without gradient G4 and $\tau_b = 1.623$ ms (*open triangles*) or $\tau_b = 1.2$ ms (tuned to $^{1}J_{HC} = 208$ Hz, *grey triangles*)

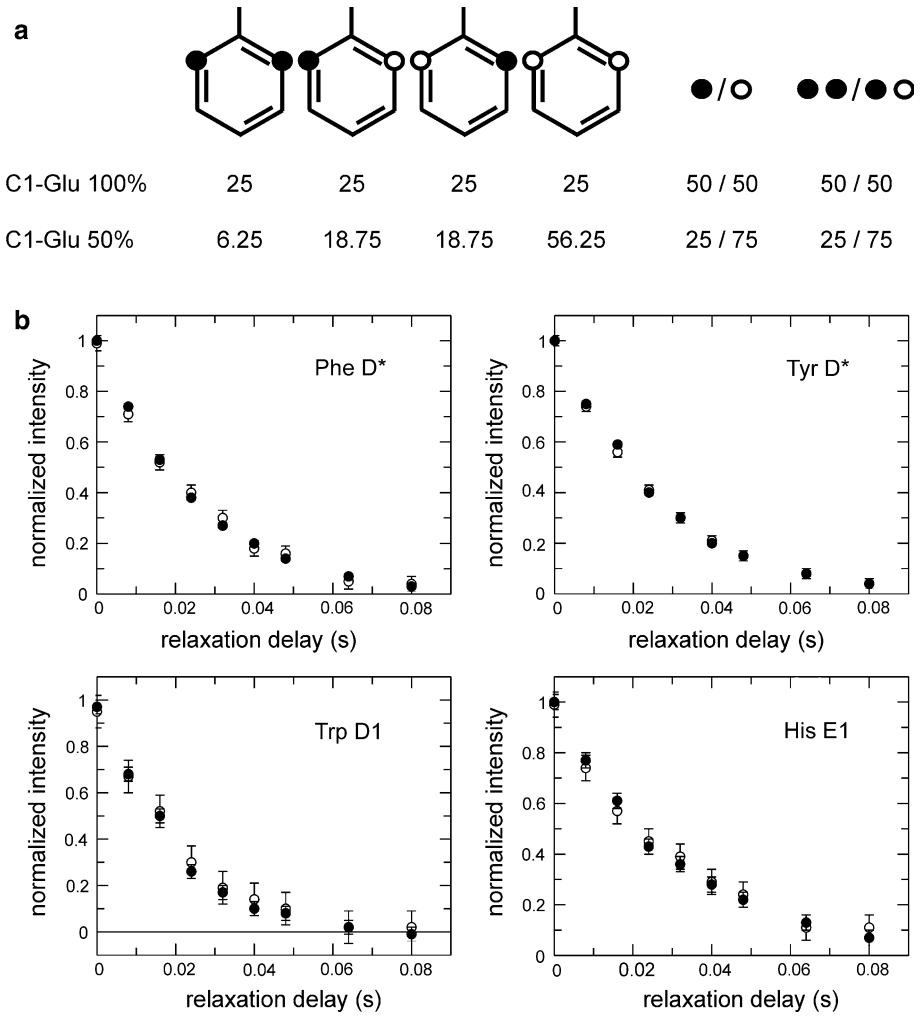

Fig. 5 Influence of two-bond ^{13}C–^{13}C *J* couplings on measured R_2 relaxation decays. **a** ^{13}C incorporation pattern in a Phe side chain resulting from labeling with 1-$^{13}C_1$-glucose. *Black circles* represent ^{13}C-labeled positions while *open circles* represent ^{12}C. The *symbols* to the *right* of the aromatic rings show the net percentages of labeled or unlabeled sites (labeled/unlabeled), and the percentages of ^{13}C sites with or without a two-bond neighbor (labeled–labeled/labeled–unlabeled). Labeling using 100 % 1-$^{13}C_1$-glucose yields 50 % ^{13}C incorporation in the Cδ positions, and 50 % of these $^{13}C\delta$ have a ^{13}C-labeled two-bond neighbour. Labeling using 50 % 1-$^{13}C_1$-glucose + 50 % $^{12}C_6$-glucose reduces the relative number of labeled carbons, as well as that of labeled two-bond neighbours, to 25 %. **b** Representative R_2 relaxation decays for different aromatic side chains in samples labeled using 100 % 1-$^{13}C_1$-glucose (*filled circles*) or 50 % 1-$^{13}C_1$-glucose + 50 % $^{12}C_6$-glucose (*open circles*)

comparison of R_1 decay curves acquired using L-optimized and standard (i.e. non-L-optimized) experiments acquired with a 3.8 s recovery delay to ensure that the aromatic ^{1}H magnetization has relaxed back to equilibrium. The relaxation decays and fitted relaxation rate constants (Fig. 3d) obtained using the L-optimized experiment are identical to those from the standard experiment, provided that ^{1}H decoupling during the relaxation delay is applied as selective pulses on the aromatics. Non-selective ^{1}H 180° pulses (in the context of L-optimization) lead to faster decays and higher apparent ^{13}C R_1 values. This result is a consequence of the intermittent inversion of water and aliphatic ^{1}H magnetization between +z and −z during the relaxation period, which makes the state of the water/aliphatic magnetization at the end of each transient dependent on the length of the relaxation period, which in turn influences the relaxation of aromatic ^{1}H spins, and hence the magnetization available for polarization transfer at the beginning of each 'scan'. The outcome is that the intensity of the monitored ^{13}C resonances will depend on the length of the relaxation period, thereby affecting the ^{13}C intensity decay curves that define the measured (apparent) relaxation rate constants; similar observations have been reported recently for ^{15}N relaxation experiments (Chen and Tjandra 2011). Therefore, it is critical in L-optimized experiments to maintain the ^{1}H magnetization of water and aliphatics along +z throughout the relaxation delay in order to ensure accurate relaxation measurements.

The results shown in Fig. 3c–d further reveal the extent to which the water and aliphatic magnetizations contribute to the increased relaxation rate of the different aromatic ^{1}H spins achieved with L-optimization. We carried out R_1 experiments in which selective ^{1}H pulses were applied to the water resonance only, thereby restricting the origin of the L-optimization effect to water spin pool. By applying non-selective ^{1}H 180° pulses during the relaxation delay we observe the type of artefacts described in the section above, but only to the extent that the relaxation of the aromatic protons is influenced by the state of the water magnetization. In this experiment, we observe artificially increased R_1 rates for atoms vicinal to sites with exchangeable protons, like Cδ2 and Cε1 in His and Cδ1 in Trp (Fig. 3c–d). By contrast, rates comparable to or slightly higher than those obtained from the standard or L-optimized experiments were observed for other sites, reflecting the signficantly reduced contribution from water in driving the relaxation of these spins. Thus, the water magnetization contributes to L-optimization mainly for ^{1}H spins situated nearby protons that exchange with water, in agreement with the higher intensity gain observed for histidines and tryptophanes (cf. Fig. 2).

L-optimized R_2 experiment

The R_2 relaxation experiment can be implemented in a straightforward fashion within the general framework presented above for the R_1 experiment (Fig. 1b). Again, it is advisable that the ^{1}H 180° pulses during the relaxation delay are selective for the aromatics in order to achieve the full benefits of L-optimization. However, the generally shorter relaxation periods needed to sample transverse

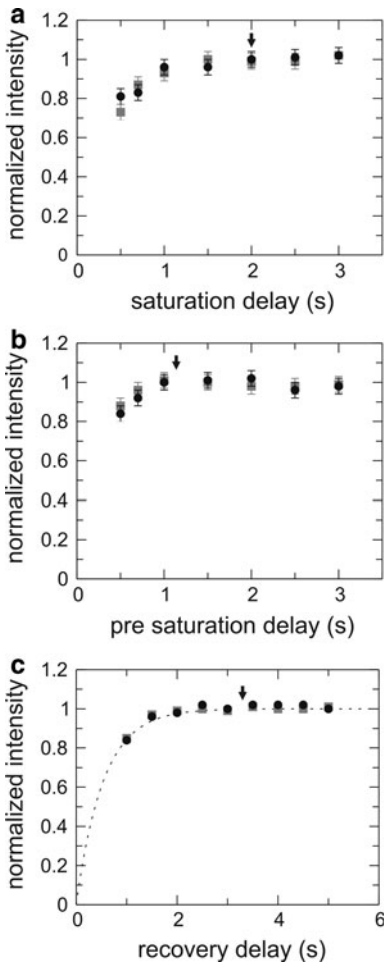

Fig. 6 Intensity build-up in the aromatic {^{1}H}–^{13}C *NOE* experiment. **a** Difference intensity (saturation experiment − reference experiment) of the {^{1}H}–^{13}C *NOE* experiment shown as a function of ^{1}H saturation time for the pulse sequences that correspond to the L-optimized (*black circles*) and non-L-optimized (*grey squares*) versions, using a constant pre-saturation delay of 4 s. **b** Difference intensity as a function of pre-saturation delays using a ^{1}H saturation time of 2 s. **c** Intensity originating from ^{13}C excitation (reference experiment) as a function of the recovery delay. Optimal delays are indicated with *black arrows*: the ^{1}H saturation period is 2 s, and the pre-saturation delay is 1.3 s. The resulting recovery delay of 3.3 s equals approximately $6/R_1$, ensuring that the ^{13}C magnetization has completely returned to equilibrium. The data represent the summed intensity of four residues: Phe149 Cδ* + Phe159 Cδ* + Tyr118 Cδ* + Tyr221 Cδ*

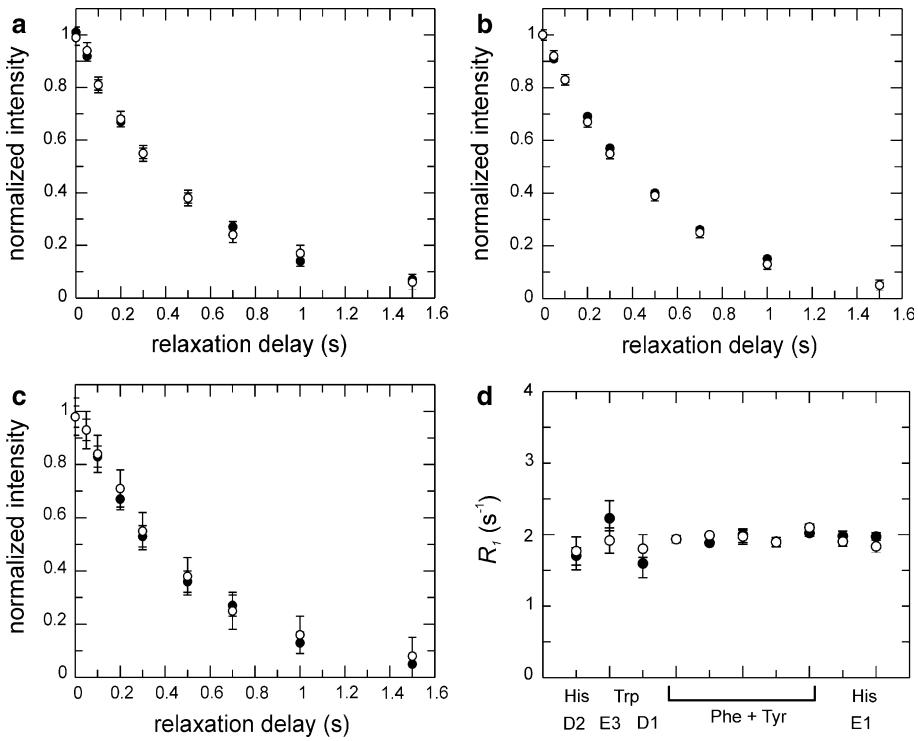

Fig. 7 Comparison of ^{13}C R_1 relaxation in partially deuterated and non-deuterated samples. **a**–**c** Representative R_1 relaxation decays measured for two Phe residues (**a**–**b**) and one His (**c**) on a partially deuterated sample (*open circles*) and non-deuterated sample (*black circles*). **d** Fitted R_1 relaxation rate constants for all ^{13}C sites characterized in Gal3C. The deuteration levels at the vicinal sites are estimated to 50–55 % for Phe and Tyr $^{1}H\varepsilon$, and 60 % for Trp $^{1}H\zeta3$ (see Table S1)

relaxation decays serve to limit the adverse effects on the ^{13}C relaxation measurements that might arise due to differential recovery of water/aliphatic magnetization as a function of the length of the relaxation period. Indeed, in the present case, L-optimized and non-L-optimized experiments yield identical R_2 rates, within errors (Fig. 4a).

The one-bond ^{1}H–^{13}C coupling constants in aromatic side chains depend on the chemical structure as follows: $^{1}J_{HC} = 155$ Hz for sites in 6-membered rings; $^{1}J_{HC} = 185$ Hz for sites in 5-membered rings with a single directly attached nitrogen, i.e. C$\delta2$ in His and C$\delta1$ in Trp; $^{1}J_{HC} = 205$ Hz for sites in 5-membered rings with two directly attached nitrogens, i.e. C$\varepsilon1$ in His. The non-uniform one-bond ^{1}H–^{13}C coupling constants require that non-refocused anti-phase magnetization be purged using a strong gradient pulse (G4 in Fig. 1b). In the absence of the purging gradient and with the refocusing delay optimized for smaller coupling constants (155–185 Hz), the residual anti-phase term gives rise to oscillations in the relaxation decay, as demonstrated for C$\varepsilon1$ in His (Fig 4b). Of course, R_2 rates can alternatively be measured in separate experiments that employ refocusing delays matching the different values of $^{1}J_{HC}$; this approach also serves the purpose to optimize the sensitivity for each class of sites.

While 1-$^{13}C_1$- and 2-$^{13}C_1$-glucose labeling effectively eradicates directly neighboring ^{13}C sites in the aromatic rings, 50 % of the labeled carbons still have another ^{13}C nucleus two bonds away. The two-bond scalar coupling is expected to be small, $^{2}J_{CC} \approx 2$–7 Hz (Kaski et al. 1996; Witanowski et al. 2007), but is practically impossible to refocus in most cases due to the narrow spectral range covered by the two resonances. We investigated the influence of the $^{2}J_{CC}$ coupling on the measured R_2 rates by comparing the results obtained from two different samples labeled using either 100 % 1-$^{13}C_1$-glucose or 50 % 1-$^{13}C_1$-glucose + 50 % $^{12}C_6$-glucose, resulting in 50 % or 25 %, respectively, of the observed carbons having a two-bond coupling partner (Fig. 5a). The resulting R_2 decays are identical within errors (Fig. 5b), thus verifying that two-bond ^{13}C-^{13}C couplings do not affect ^{13}C R_2 measurements to any appreciable extent.

{^{1}H}–^{13}C *NOE* experiment

The {^{1}H}–^{13}C *NOE* saturation and reference experiments were optimized in a straightforward fashion by finding the shortest possible saturation and recycle periods that still provide full magnetization transfer and recovery. Since the length of the *NOE* reference experiment is governed by the recovery of the heteronucleus (^{13}C in the present case), L-optimization offers little or no advantage for a medium-sized protein like Gal3C, as shown in Fig. 6. Still, selective ^{1}H pulses for proton saturation are beneficial in order to achieve equal water suppression in both the saturation and reference experiments. For Gal3C, a ^{1}H saturation period of 2 s is sufficient to achieve complete *NOE* transfer (Fig. 6a). This value is in agreement with the data shown in Fig. 2a, demonstrating that the chosen length of the saturation period is close to $6 \cdot T_1$ for the aromatic protons. As shown in Fig. 6b, a pre-saturation delay of 1.3 s guarantees

full recovery of the ^{1}H magnetization. The recycle delay of the reference experiment is set to 3.3 s (approximately $6 \cdot T_1$ for aromatic ^{13}C spins), which ensures that the ^{13}C magnetization has relaxed back to equilibrium (Fig. 6c).

Vicinal and remote protons do not affect the relaxation of aromatic ^{13}C spins

The interpretation of the ^{13}C relaxation rates in terms of models describing the motion of the aromatic rings is greatly simplified if the relaxation is dominated by the CSA and dipolar interaction with the covalently attached proton (bond length 1.08 Å). We established that there is no detectable influence from ^{1}H spins located near the aromatic ^{1}H–^{13}C moieties of interest. The vicinal protons are expected to be the closest ones, at a distance of 2.14 Å in the case of Phe and Tyr. The dipolar interaction with the vicinal protons is reduced by a factor of approximately $(1.08/2.14)^6 = 1.7$ %, compared to that of the covalently attached proton; consequently, relaxation effects due to vicinal or other neighboring protons are expected to be small. We verified the theroretical prediction by comparing ^{13}C relaxation rates measured on samples that were either fully protonated or partially deuterated to a level of 50–60 % at the vicinal sites (Table S1) and approximately 50 % on average. As shown in Fig. 7, there are no discernable differences in ^{13}C relaxation between these two samples. Thus, we conclude that relaxation measurements on specifically ^{13}C labeled aromatic side chains are unaffected by remote protons.

Conclusions

We have shown that L-optimization increases the sensitivity (defined in terms of signal-to-noise per unit time) of ^{13}C relaxation experiments for aromatic side chains by at least 10–35 %. This level of S/N enhancement was attained for a relatively small protein of 16 kDa at a static magnetic field strength of 11.7 T. Significantly higher S/N enhancement are expected for bigger proteins and higher static magnetic field strengths, which both result in slower ^{1}H R_1 relaxation rates and therefore makes L-optimization increasingly advantageous. Proteins larger in size than approximately 25–30 kDa (at 25 °C) benefit further from TROSY-based ^{13}C chemical shift evolution. Furthermore, we demonstrate that the relaxation measurements are not significantly affected by potential complications due to residual two-bond ^{13}C–^{13}C scalar couplings or dipolar interactions with neighboring ^{1}H spins. Precise control of the water and aliphatic ^{1}H magnetizations enables accurate measurements of ^{13}C relaxation rate constants using L-optimized pulse sequences.

Acknowledgments This work was supported by the Swedish Research Council (621-2010-4912), the FLÄK Research School for Pharmaceutical Sciences at Lund University, the Göran Gustafsson Foundation for Research in Natural Sciences and Medicine, and the Knut and Alice Wallenberg Foundation. U.W. was supported by an EMBO long-term fellowship.

References

Bartlett GJ, Porter CT, Borkakoti N, Thornton JM (2002) Analysis of catalytic residues in enzyme active sites. J Mol Biol 324: 105–121

Berglund H, Baumann H, Knapp S, Ladenstein R, Härd T (1995) Flexibility of an arginine side chain at a DNA-protein interface. J Am Chem Soc 117:12883–12884

Birtalan S, Fisher RD, Sidhu SS (2010) The functional capacity of the natural amino acids for molecular recognition. Mol BioSyst 6: 1186–1194

Bogan AA, Thorn KS (1998) Anatomy of hot spots in protein interfaces. J Mol Biol 280:1–9

Boyd J (1995) Measurement of ^{15}N relaxation data from the side chains of asparagine and glutamine residues in proteins. J Magn Reson B 107:279–285

Boyer JA, Lee AL (2008) Monitoring aromatic picosecond to nanosecond dynamics in proteins via 13C relaxation: expanding perturbation mapping of the rigidifying core mutation V54A in Eglin C. Biochemistry 47:4876–4886

Cavanagh J, Fairbrother WJ, Palmer AG, Rance M, Skelton NJ (2007) Protein NMR spectroscopy: principles and practice. Elsevier Academic Press, San Diego

Chen K, Tjandra N (2011) Water proton spin saturation affects measured protein backbone 15N spin relaxation rates. J Magn Reson 213:151–157

Delaglio F, Grzesiek S, Vuister GW, Zhu G, Pfeifer J, Bax A (1995) NMRPipe: a multidimensional spectral processing system based on UNIX pipes. J Biomol NMR 6:277–293

Diehl C, Genheden S, Modig K, Ryde U, Akke M (2009) Conformational entropy changes upon lactose binding to the carbohydrate recognition domain of galectin-3. J Biomol NMR 45: 157–169

Diehl C, Engström O, Delaine T, Håkansson M, Genheden S, Modig K, Leffler H, Ryde U, Nilsson UJ, Akke M (2010) Protein flexibility and conformational entropy in ligand design targeting the carbohydrate recognition domain of galectin-3. J Am Chem Soc 132:14577–14589

Eletsky A, Atreya HS, Liu GH, Szyperski T (2005) Probing structure and functional dynamics of (large) proteins with aromatic rings: L-GFT-TROSY (4,3)D HCCHNMR spectroscopy. J Am Chem Soc 127:14578–14579

Ferrage F, Piserchio A, Cowburn D, Ghose R (2008) On the measurement of N-15–{H-1} nuclear Overhauser effects. J Magn Reson 192:302–313

Ferrage F, Cowburn D, Ghose R (2009) Accurate sampling of high-frequency motions in proteins by steady-state N-15–{H-1} nuclear Overhauser effect measurements in the presence of cross-correlated relaxation. J Am Chem Soc 131:6048–6049

Geen H, Freeman R (1991) Band-selective radiofrequency pulses. J Magn Reson 93:93–141

Igumenova TI, Frederick KK, Wand AJ (2006) Characterization of the fast dynamics of protein amino acid side chains using NMR relaxation in solution. Chem Rev 106:1672–1699

Ishima R, Petkova AP, Louis JM, Torchia DA (2001) Comparison of methyl rotation axis order parameters derived from model-free analyses of H-2 and C-13 longitudinal and transverse relaxation rates measured in the same protein sample. J Am Chem Soc 123:6164–6171

Iwahara J, Jung YS, Clore GM (2007) Heteronuclear NMR spectroscopy for lysine NH3 groups in proteins: unique effect of water exchange on N-15 transverse relaxation. J Am Chem Soc 129:2971–2980

Jarymowycz VA, Stone MJ (2006) Fast time scale dynamics of protein backbones: NMR relaxation methods, applications, and functional consequences. Chem Rev 106:1624–1671

Johnson BA, Blevins RA (1994) NMRView: a computer program for the visualization and analysis of NMR data. J Biomol NMR 4:603–614

Kaski J, Vaara J, Jokisaari J (1996) C-13–C-13 spin–spin coupling tensors in benzene as determined experimentally by liquid crystal NMR and theoretically by ab initio calculations. J Am Chem Soc 118:8879–8886

Kay LE, Keifer P, Saarinen T (1992) Pure absorption gradient enhanced heteronuclear single quantum correlation spectroscopy with improved sensitivity. J Am Chem Soc 114:10663–10665

Kupce E, Boyd J, Campbell ID (1995) Short selective pulses for biochemical applications. J Magn Reson B 106:300–303

Levy RM, Sheridan RP (1983) Combined effect of restricted rotational diffusion plus jumps on nuclear magnetic resonance and fluorescence probes of aromatic ring motions in proteins. Biophys J 41:217–221

Lo Conte L, Chothia C, Janin J (1999) The atomic structure of protein–protein recognition sites. J Mol Biol 285:2177–2198

Lundström P, Teilum K, Carstensen T, Bezsonova I, Wiesner S, Hansen F, Religa TL, Akke M, Kay LE (2007) Fractional ^{13}C enrichment of isolated carbons using [1-^{13}C]- or [2-^{13}C]-glucose facilitates the accurate measurement of dynamics at backbone Ca and side-chain methyl positions in proteins. J Biomol NMR 38:199–222

Millet O, Muhandiram DR, Skrynnikov NR, Kay LE (2002) Deuterium spin probes of side-chain dynamics in proteins. 1. Measurement of five relaxation rates per deuteron in ^{13}C-labeled and fractionally ^{2}H-enriched proteins in solution. J Am Chem Soc 124:6439–6448

Muhandiram DR, Yamazaki T, Sykes BD, Kay LE (1995) Measurement of ^{2}H T_1 and $T_{1\rho}$ relaxation times in uniformly ^{13}C-labeled and fractionally ^{2}H-labeled proteins in solution. J Am Chem Soc 117:11536–11544

Palmer AG (2004) NMR characterization of the dynamics of biomacromolecules. Chem Rev 104:3623–3640

Palmer AG, Cavanagh J, Wright PE, Rance M (1991) Sensitivity improvement in proton-detected two-dimensional heteronuclear correlation NMR spectroscopy. J Magn Reson 93:151–170

Palmer AG, Hochstrasser RA, Millar DP, Rance M, Wright PE (1993) Characterization of amino acid side chain dynamics in a zinc-finger peptide using ^{13}C NMR spectroscopy and time-resolved fluorescence spectroscopy. J Am Chem Soc 115:6333–6345

Paquin R, Ferrage F, Mulder FAA, Akke M, Bodenhausen G (2008) Multiple-timescale dynamics of side-chain carboxyl and carbonyl groups in proteins by C-13 nuclear spin relaxation. J Am Chem Soc 130:15805+

Pervushin K, Riek R, Wider G, Wüthrich K (1997) Attenuated T_2 relaxation by mutual cancellation of dipole–dipole coupling and chemical shift anisotropy indicates an avenue to NMR structures of very large biological macromolecules in solution. Proc Natl Acad Sci USA 94:12366–12371

Pervushin K, Riek R, Wider G, Wüthrich K (1998) Transverse relaxation-optimized spectroscopy (TROSY) for NMR studies of aromatic spin systems in ^{13}C-labeled proteins. J Am Chem Soc 120:6394–6400

Pervushin K, Vogeli B, Eletsky A (2002) Longitudinal H-1 relaxation optimization in TROSY NMR spectroscopy. J Am Chem Soc 124:12898–12902

Sapienza PJ, Mauldin RV, Lee AL (2011) Multi-timescale dynamics study of FKBP12 along the rapamycin-mTOR binding coordinate. J Mol Biol 405:378–394

Separovic F, Hayamizu K, Smith R, Cornell BA (1991) C-13 chemical-shift tensor of L-tryptophan and its application to polypeptide structure determination. Chem Phys Lett 181: 157–162

Separovic F, Ashida J, Woolf T, Smith R, Terao T (1999) Determination of chemical shielding tensor of an indole carbon and application to tryptophan orientation of a membrane peptide. Chem Phys Lett 303:493–498

Sklenar V, Piotto M, Leppik R, Saudek V (1993) Gradient-tailored water suppression for H-1–N-15 Hsqc experiments optimized to retain full sensitivity. J Magn Reson A 102:241–245

Teilum K, Brath U, Lundström P, Akke M (2006) Biosynthetic 13C labeling of aromatic side-chains in proteins for NMR relaxation measurements. J Am Chem Soc 128:2506–2507

Veeman WS (1984) Carbon-13 chemical shift anisotropy. Prog NMR Spectrosc 16:193–235

Witanowski M, Kamienska-Trela K, Biedrzycka Z (2007) Indirect carbon–carbon couplings across one, two and three bonds in substituted benzenes: experiment and theory. J Mol Struct 844: 13–20

Wüthrich K, Wagner G (1975) NMR investigations of the dynamics of the aromatic amino acid residues in the basic pancreatic trypsin inhibitor. FEBS Lett 50:265–268

Yang DW, Mittermaier A, Mok YK, Kay LE (1998) A study of protein side-chain dynamics from new H-2 auto-correlation and C-13 cross-correlation NMR experiments: application to the N-terminal SH3 domain from drk. J Mol Biol 276:939–954

Yip GNB, Zuiderweg ERP (2004) A phase cycle scheme that significantly suppresses offset-dependent artifacts in the R-2-CPMG N-15 relaxation experiment. J Magn Reson 171:25–36